Processing and Application of Ceramics 11 [1] (2017) 67–74
DOI: 10.2298/PAC1701067A

Effect of sintering temperature on the microstructure and ionic conductivity of $Ce_{0.8}Sm_{0.1}Ba_{0.1}O_{2-\delta}$ electrolyte

Mustafa Anwar[1,2], Muhammed Ali S.A.[1], Abdalla M. Abdalla[3], Mahendra Rao Somalu[1], Andanastuti Muchtar[1,4,*]

[1]*Fuel Cell Institute, Universiti Kebangsaan Malaysia, 43600, UKM Bangi, Selangor Darul Ehsan, Malaysia*
[2]*U.S.-Pakistan Center for Advanced Studies in Energy (USPCAS-E), National University of Sciences and Technology, 44000, H-12, Islamabad, Pakistan*
[3]*Faculty of Integrated Technologies, Universiti Brunei Darussalam, JalanTunku Link, Gadong BE 1410, Brunei Darussalam*
[4]*Department of Mechanical and Materials Engineering, Faculty of Engineering and Built Environment, Universiti Kebangsaan Malaysia, 43600, UKM Bangi, Selangor Darul Ehsan, Malaysia*

Received 29 September 2016; Received in revised 2 January 2017; Accepted 7 March 2017

Abstract

This study investigated the effects of sintering temperature on the microstructure and ionic conductivity of co-doped ceria electrolyte with barium and samarium as dopants. The electrolyte ($Ce_{0.8}Sm_{0.1}Ba_{0.1}O_{2-\delta}$) powder was synthesized using the citric acid-nitrate combustion method and calcined at 900 °C for 5 h. The calcined electrolyte exhibited a cubic fluorite crystal structure with some impurity phases. The calcined powder was then pressed into cylindrical pellets using uniaxial die-pressing. The pellets were sintered at three different temperatures, i.e., 1200, 1300 and 1400 °C for 5 h. Microstructural analysis of the pellets showed that the average grain size increased with the increase in sintering temperature. The sintered densities of the pellets were measured by Archimedes' method, and the relative density values were within the range of 78 %TD to 87 %TD as the sintering temperature increased from 1200 to 1400 °C. Electrochemical impedance spectroscopy analysis showed that conductivity increased with the increase in sintering temperature, but no considerable change in conductivity was observed for the pellets sintered at 1300 and 1400 °C. The results revealed that the electrolyte pellet sintered at 1300 °C exhibited the ionic conductivity of 0.005 S/cm with lowest activation energy of 0.7275 eV.

Keywords: *CeO_2, doping, sintering, microstructure, ionic conductivity*

I. Introduction

Solid oxide fuel cells (SOFCs) are highly efficient, fuel flexible and environmentally friendly devices that directly convert the chemical energy of fuels to an electrical energy through electrochemical reactions [1]. Yttria-stabilized zirconia (YSZ) is the most commonly used electrolyte material for conventional SOFCs. Traditional SOFCs exhibit better performance only at high operating temperature (800 to 1000 °C) because YSZ requires high temperature for sufficient ionic conductivity. Currently, one of the major challenges is to reduce the operating temperature of SOFCs because high temperatures cause various issues, e.g., material degradation, expensive sealants and interconnects, long start-up/shutdown time, and thermal stress. The operating temperature of SOFCs can be lowered by developing new electrolytes that exhibit high ionic conductivity either at intermediate temperature (600 to 800 °C) or low temperature (< 600 °C). In this context, doped ceria-based materials show high ionic conductivity at 500 to 800 °C and they are used as electrolytes for intermediate-temperature SOFCs (ITSOFCs) [2].

Among doped ceria-based electrolytes, samarium-doped ceria (SDC, $Ce_{0.8}Sm_{0.2}O_{1.9}$) exhibits the highest ionic conductivity [3]. Moreover, the ionic conductiv-

* Corresponding author: tel: +603 89213895,
fax: +603 89252699, e-mail: *muchtar@ukm.edu.my*

ity of SDC can be further enhanced by co-doping. Co-doping refers to the addition of two aliovalent cations into the host (ceria) lattice. This approach is useful in improving the electrical properties of various electrolytes [4,5]. Studies [6,7] have proven the high values of ionic conductivity for co-doped SDC compared with the values for singly-doped SDC. In those studies, co-doping is usually conducted with alkaline earth metals, such as Sr^{2+} and Ca^{2+}, or with rare-earth elements, such as Nd^{3+} and La^{3+}. The co-doping with alkaline earth elements is advantageous because of low cost and extensive availability. Co-doped SDC electrolyte with Ba^{2+} ($Ce_{0.8}Sm_{0.15}Ba_{0.05}O_{2-\delta}$) shows an oxygen ion conductivity of 0.360 S/cm at 800 °C [7]. However, available literature on $Ce_{0.8}Sm_{0.2-x}Ba_xO_{2-\delta}$ is scarce. Therefore, the current paper reports the synthesis and characterization of $Ce_{0.8}Sm_{0.1}Ba_{0.1}O_{2-\delta}$ electrolyte material.

Synthesis conditions, especially sintering temperature, significantly affect the microstructure and electrical conductivity of doped ceria-based electrolytes [8,9]. Therefore, the main objective of this study is to determine the effects of sintering temperature on the microstructure and ionic conductivity of $Ce_{0.8}Sm_{0.1}Ba_{0.1}O_{2-\delta}$ electrolyte. The co-doped electrolyte was synthesized using the citric acid-nitrate combustion method and sintered at three different temperatures. The microstructure analysis and ionic conductivity were carried out and then compared.

II. Experimental

$Ce_{0.8}Sm_{0.1}Ba_{0.1}O_{2-\delta}$ (BSDC) was synthesized by citric acid-nitrate combustion method. Analytical-grade cerium nitrate hexahydrate [$Ce(NO_3)_3{\cdot}6\,H_2O$; 99%], samarium nitrate hexahydrate [$Sm(NO_3)_3{\cdot}6\,H_2O$; 99%], and barium nitrate [$Ba(NO_3)_2$; 99%] were used as precursors; whereas citric acid was used as fuel for combustion. All the chemicals were purchased from Sigma Aldrich, Malaysia, and used without further purification.

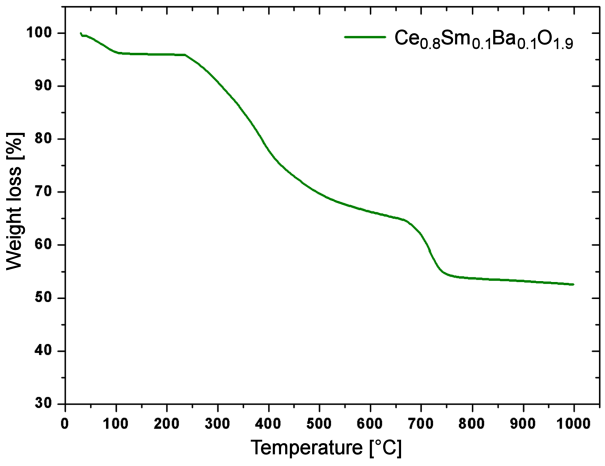

Figure 1. Thermogravimetric plot of uncalcined BSDC powder

2.1. Sample preparation

Stoichiometric amounts of $Ce(NO_3)_3{\cdot}6\,H_2O$, $Sm(NO_3)_3{\cdot}6\,H_2O$, $Ba(NO_3)_2$, and citric acid were dissolved in deionized water with magnetic stirring. Total metal ion-to-citric acid molar ratio was 1 : 1.5. The solution mixture was heated to 80 °C for water to evaporate, forming a viscous gel. The gel was heated continuously at a lower temperature (80 °C) to initiate combustion, forming a pale yellow ash. The resulting ash was placed overnight in a pre-heated oven at 120 °C (12 h) to dry and to complete the combustion reaction. The dried powder was calcined at 900 °C for 5 h to obtain the desired single phase BSDC powder. The BSDC powder was then cold-pressed at 50 MPa into cylindrical pellets with diameter of 13 mm and thickness of 1 mm using a uniaxial die-press. The as-prepared green pellets were sintered for densification at 1200, 1300 and 1400 °C for 5 h in air.

2.2. Characterization

Thermal behaviour of the dried powder was investigated using thermogravimetric analysis (TGA, PerkinElmer, STA 6000, USA) in the temperature range of 30 to 1000 °C at a heating rate of 10 °C/min in flowing nitrogen with a flow rate of 25 ml/min. Phase characterization, theoretical density, and crystallite size of the calcined powder was determined at room temperature by X-ray diffraction (XRD, Bruker AXS, D8-Advance, Germany) with Cu Kα (λ = 0.15406 nm) radiation at a scan rate of 0.025°/step. The specific surface area of the calcined electrolyte was measured by surface area and porosimetry system (Micromeritics, ASAP 2020, USA) employing Brunauer-Emmett-Teller (BET) technique.

The sintered pellets were polished by 240-, 800- and 1200-grit sand papers to achieve a similar thickness and to obtain a smooth surface. The apparent densities of the pellets were calculated by Archimedes' method, and their morphology and microstructure were observed by field-emission scanning electron microscopy (FESEM, Zeiss Merlin, Germany). A silver paint from RS Components Ltd. UK was coated on both sides of the polished pellets for electrical measurements. After coating, silver paste was dried at 150 °C for 40 minutes. The electrical conductivities were measured by electrochemical impedance spectroscopy (EIS) using potentiostat coupled with a frequency response analyser (Eco Chemie, Autolab 302, Netherlands). The conductivities were found within the temperature range of 600 to 800 °C with an interval of 50 °C and a frequency range of 0.1 Hz to 1 MHz under a low-amplitude sinusoidal voltage of 10 mV.

III. Results and discussion

3.1. Thermogravimetric analysis

Figure 1 shows the thermogravimetric analysis plot of the uncalcined powder. The total weight loss was ~45%. An initial weight loss of approximately 4% was

observed between 50 to 130 °C due to the evaporation of the absorbed moisture. The major weight loss of approximately 41% was observed between 250 to 750 °C due to the decomposition of nitrates and organic fuel into different gases, such as nitrogen, carbon dioxide, and water vapours. Moreover, the crystallization of co-doped ceria solution gradually started at 450 °C [6,10]. No remarkable change in weight loss was observed after 750 °C, which demonstrated the formation of pure crystalline phase in the co-doped ceria solid solution.

3.2. X-ray diffraction analysis

The XRD pattern of the calcined electrolyte powder is shown in Fig. 2. The search and match analysis was carried out by X'Pert High Score Plus software and all the major peaks match the cubic fluorite crystal structure of pure cerianite (CeO_2, space group *Fm-3m* (225), ICDD Reference Code: 96-900-9009). However, some low intensities peaks are observed at ~25°, ~41°, and 51°. The peak at ~25° is designated to $BaO_{1.3}$, whereas the peaks at ~41° and ~51° are designated to $BaCeO_3$ [7].

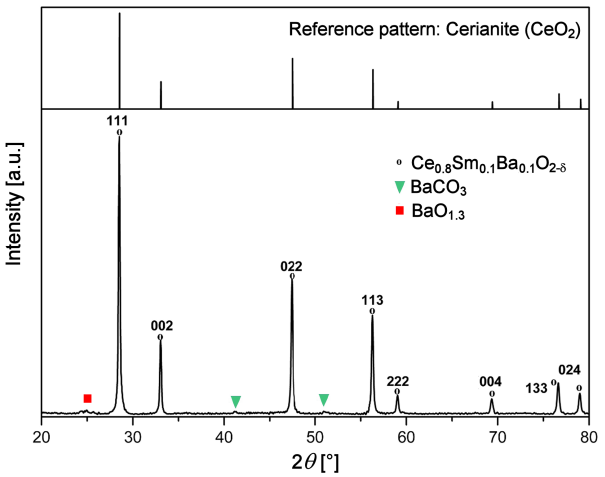

Figure 2. XRD pattern of BSDC powder calcined at 900 °C for 5 h

The sharpness in the XRD peaks indicated that the electrolyte is perfectly crystalline after calcination, which corresponded to the TGA results. The lattice parameter of BSDC electrolyte was calculated using Eqs. 1 and 2 for all the peaks and the result was 5.419 Å, which is greater than that of cerianite reference, i.e., 5.411 Å [11]. The increase in the lattice parameter was due to the large ionic radii of Sm^{3+} and Ba^{2+} compared with the host ion (Ce^{4+}).

$$a = d\sqrt{h^2 + k^2 + l^2} \tag{1}$$

$$d = \frac{\lambda}{2\sin\theta} \tag{2}$$

where a is the lattice parameter, d is the planar spacing, hkl are the Miller indices, λ is the wavelength of X-rays (1.5406 Å), and θ is the peak position. From the value of lattice parameter, the theoretical density (ρ_{Th}) of the BSDC electrolyte was calculated by using following equation:

$$\rho_{Th} = \frac{4 \cdot MW_{BSDC}}{N_A \cdot a} \tag{3}$$

where MW_{BSDC} is molecular weight of BSDC electrolyte and N_A is Avogadro's number. The calculated theoretical density of 7.149 g/cm^3 will be further used to determine the relative density of the sintered electrolyte.

Due to the increase in lattice parameter of BSDC electrolyte the value of lattice strain was calculated using the following equation [12]:

$$\varepsilon = \frac{a_{BSDC} - a_{CeO_2}}{a_{CeO_2}} \tag{4}$$

where a_{BSDC} is the lattice parameter of co-doped ceria electrolyte and a_{CeO_2} is the lattice parameter of cerianite. The value of lattice strain was 0.148%.

The crystallite sizes of the two major peaks (111 and 022) were calculated using Scherrer's formula:

$$D_{XRD} = \frac{0.9\lambda}{\beta\cos\theta} \tag{5}$$

where D_{XRD} is the crystallite size, λ is the wavelength of Cu Kα rays (0.15406 nm), β is the corrected full width at half maximum, and θ is the peak position. The particle size (D_{BET}) was calculated using following equation [13,14]:

$$D_{BET} = \frac{6000}{\rho_{Th} \cdot S_v} \tag{6}$$

where D_{BET} is the particle size, ρ_{Th} is the theoretical density and S_v is the specific surface area.

The estimated crystallite sizes from the two major peaks (111 and 022) were 67 and 63 nm, respectively. However, the particle size (D_{BET}) calculated from the specific surface area measurement was 189 nm. This indicated the partial sintering of the active nanocrystallites to form agglomerates [15] and the index of extent of agglomeration ($\psi = D_{BET}/D_{XRD}$) was 2.80. For SDC-based electrolytes, the reported value of this index ranges from 1.08 to 4.7 [13,14]. Table 1 shows the values of different parameters that were calculated based on the XRD and BET analyses.

Table 1. Lattice parameter (a), theoretical density (ρ_{Th}), crystallite size (D_{XRD}), specific surface area (S_v), particle size (D_{BET}) and $\psi = D_{BET}/D_{XRD}$ of BSDC calcined powder obtained from XRD and BET

Composition	a [Å]	ρ_{Th} [g/cm^3]	D_{XRD} [nm]	S_v [m^2/g]	D_{BET} [nm]	ψ
$Ce_{0.8}Sm_{0.1}Ba_{0.1}O_{2-\delta}$	5.419	7.149	67.2	4.446	188.68	2.807

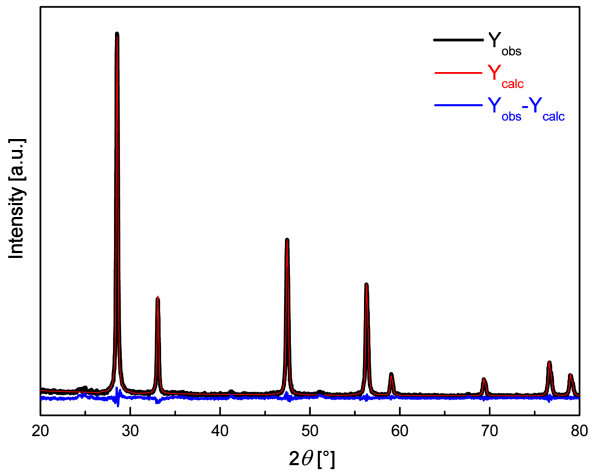

Figure 3. Rietveld analysis of BSDC electrolyte calcined at 900 °C for 5 h

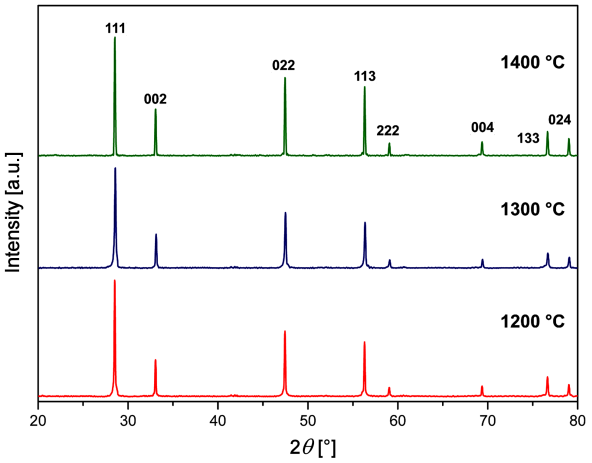

Figure 4. XRD patterns of BSDC pellets sintered at 1200 °C, 1300 °C and 1400 °C for 5 h

The structural refinement of the XRD pattern of calcined BSDC electrolyte was carried out by Rietveld analysis and is shown in Fig. 3. The calculated pattern is comparable with the observed pattern and the difference between the two patterns is approximately a straight line. The value of lattice parameter obtained after the refinement was 5.416 Å, which was comparable to the calculated value i.e., 5.419 Å. The values of the different agreement indices, such as expected *R*-factor (R_{exp}), weighted profile *R*-factor (R_{wp}), and Bragg *R*-factor (R_{Bragg}) were 7.69794, 11.47634 and 4.20, respectively; whereas the goodness of fit was 1.49083.

Figure 4 shows the XRD patterns of BSDC pellets sintered at 1200, 1300 and 1400 °C for 5 h. All peaks are designated to the cubic fluorite crystal structure of cerianite (CeO_2), and no impurity phases are present. The lattice parameters of the sintered pellets were calculated from Eqs. 1 and 2 and found to be ~5.415 Å for all the sintered pellets.

3.3. Densification and microstructure

The sintered and relative densities of all the pellets are given in Table 2. Sintered densities (ρ_s) were calculated by Archimedes' method using deionized water:

$$\rho_s = \frac{M_d \cdot \rho_w}{M_{sat} \cdot M_{sus}} \tag{7}$$

where M_d is the dry weight of pellet, ρ_w is the density of deionized water, M_{sat} is the saturated weight, and M_{sus} shows the suspended weight of pellets. The relative densities were determined by following equation:

$$\rho_r = \frac{\rho_s}{\rho_{Th}} 100 \tag{8}$$

where ρ_s is the sintered density of electrolyte pellet and ρ_{Th} is the theoretical density of an electrolyte. The sintered densities and consequent relative densities of the sintered pellets increased as sintering temperature increased. Relative densities were within the range of 78 %TD to 87 %TD as the sintering temperature increased from 1200 to 1400 °C.

The FESEM images of the surfaces and cross-sections of sintered pellets at three different temperatures are shown in Figs. 5 and 6. These images show that porosity decreases and, consequently, densification increases with the increase in sintering temperature. An increase in the grain growth was also observed as sintering temperature increased, because duirng densification the large grains are produced at the cost of smaller ones [16]. The average grain size was less than 1 μm for the pellet sintered at 1200 °C, whereas for 1300 and 1400 °C, the average grain size ranged from 1.7 to 2.8 μm and 3 to 4.7 μm, respectively. From Fig. 5b,c, grain size inhomogeneity was observed and grain size distribution was not uniform especially at higher sintering temperatures (1300 and 1400 °C). During sintering, two main processes occurred, i.e., densification and coarsening. The increase in the grain size from 1.7 μm to 4.7 μm shows that coarsening occurred. Figure 5b,c shows that the abnormal grain growth occurred which caused the pores to be trapped inside the grains and difficult to remove. This limited the relative density even at higher sintering temperatures [17]. However, the densification of the BSDC electrolyte system can be enhanced by prolonging the sintering time to control the abnormal grain growth and by introducing sintering aids [17–19].

Table 2. Values of sintered and relative densities at different sintering temperatures

Sintering temperature [°C]	Sintered density (ρ_s) [g/cm^3]	Relative density (ρ_s/ρ_{Th}) [%TD]
1200	5.635	78.834
1300	6.104	85.389
1400	6.214	86.921

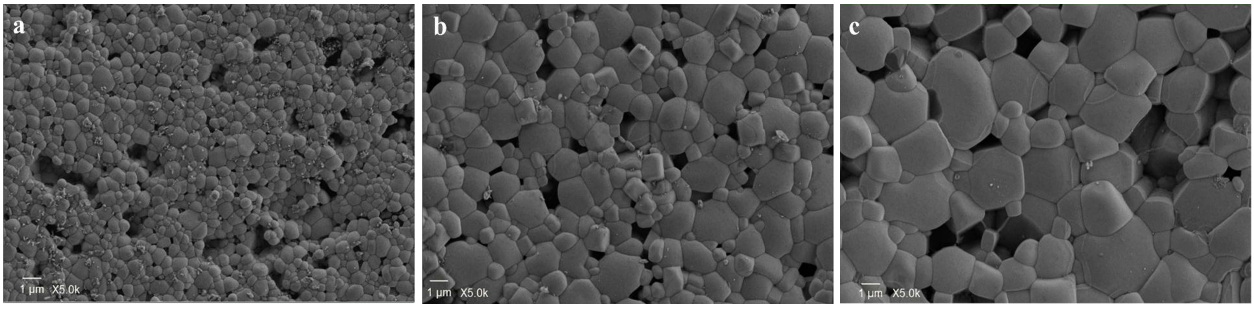

Figure 5. FESEM images of the surfaces of BSDC pellets sintered at: a) 1200 °C, b) 1300 °C and c) 1400 °C

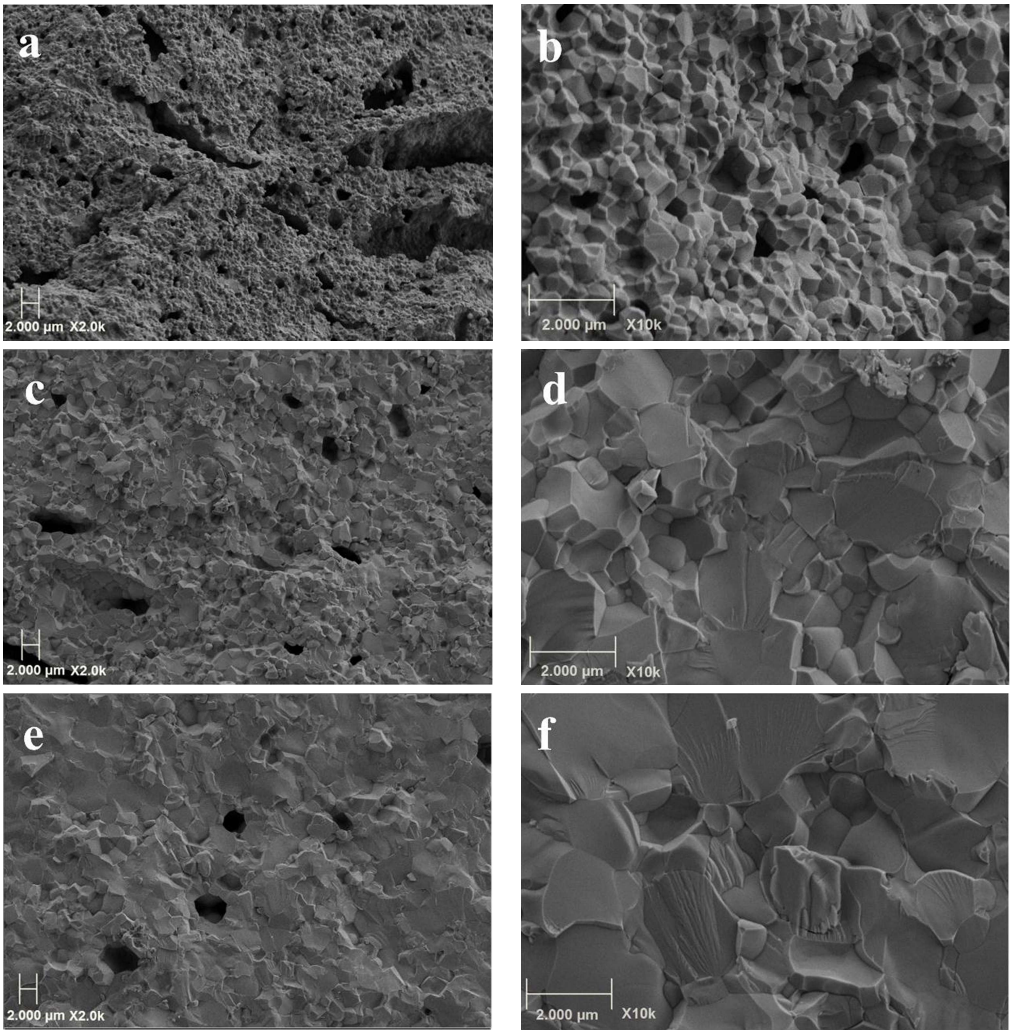

Figure 6. Cross-sectional images of BSDC pellets sintered at (a and b) 1200 °C, (c and d) 1300 °C, and (e and f) 1400 °C

3.4. Electrical properties

A typical Nyquist plot of a solid ceramic electrolyte shows three semi-circles wherein the high frequency arc represents the grain or bulk resistance (R_b), intermediate frequency arc represents the grain-boundary resistance (R_{gb}) and low frequency arc shows electrode or electrode/electrolyte interface resistance (R_{el}) [3]. The electrode or electrode/electrolyte interface resistance was not in the scope of this study.

The Nyquist plots of the sintered BSDC electrolyte pellets measured at 800 °C and 650 °C are shown in Figs. 7 and 8, respectively. At 650 °C (Fig. 8), two semi-circles appeared for all three sintered pellets. The first semi-circle showed the grain-boundary contribution, whereas the second semi-circle showed the electrode resistance. However, at 800 °C (Fig. 7), two semi-circles appeared only for the samples sintered at 1200 and 1300 °C; for the sample sintered at 1300 °C, the first circle appeared at 60.62 kHz. Therefore, this first semi-circle was attributed to the electrode resistance, because the responses of grain and grain-boundary contributions usually appear at frequencies greater than 100 kHz [20]. Thus, as the temperature increased from 650 to 800 °C, the arcs shifted towards the low frequency regime; and

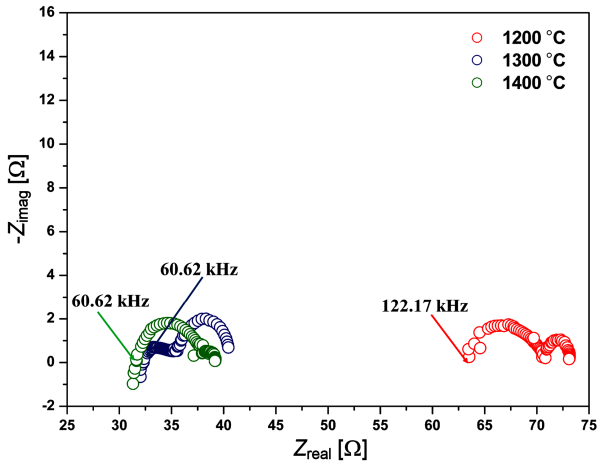

Figure 7. Nyquist plots of BSDC sintered pellets measured at 800 °C

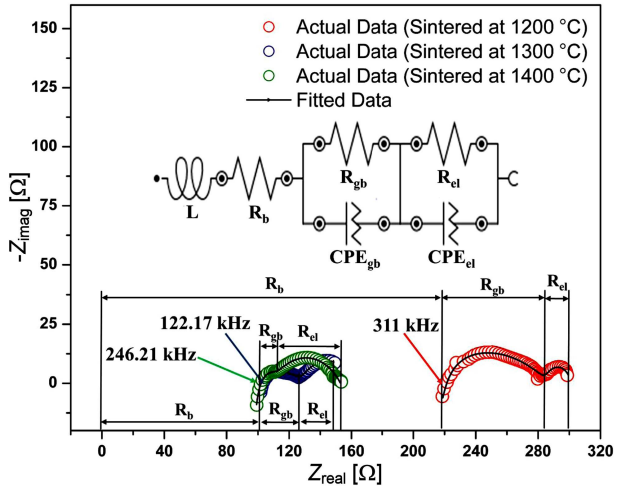

Figure 8. Impedance spectra, circuit fitting and equivalent circuit models of BSDC sintered pellets measured at 650 °C

at 800 °C the grain-boundary circle dissappeared for the electrolyte pellets sintered at 1300 and 1400 °C. This was due to the smaller time constant associated with the grain-boundary resistance compared with the electrode or electrode/electrolyte interface resistances [21,22]. Moreover, as temperature increased from 650 to 800 °C, distinguishing between the bulk and grain-boundary resistances for the samples sintered at 1300 and 1400 °C became difficult. This was because of the identical relaxation times of oxygen vacancies both inside the grain and within the grain-boundaries [22].

The total resistance (R_t) of the sintered electrolyte pellet is the sum of bulk and grain-boundary resistances, i.e, $R_t = R_b + R_{gb}$. In order to find the exact values of R_b and R_{gb}, the equivalent circuit $LR_b(R_{gb}CPE_{gb})(R_{el}CPE_{el})$ was drawn by fitting the impedance spectra using NOVA 1.10 software, which is shown in Fig. 8. In the equivalent circuit, L represents the inductive reactance due to the leads/wires and equipment, and it usually appears at high frequencies (~0.5 MHz to 1 MHz); whereas, CPE means 'constant phase element' and shows the time-dependency of capacitive elements.

Ionic conductivity (σ) of all the sintered pellets was measured using the following equation:

$$\sigma = \frac{1}{R_t} \cdot \frac{L}{A} \tag{9}$$

where $R_t = (R_b + R_{gb})$ represents the total resistance, L and A represent the thickness and area of the sintered pellets, respectively. Arrhenius' law was used to represent the relationship between conductivity and temperature:

$$\sigma = \frac{\sigma_0}{T} \exp\left(\frac{-E_a}{k \cdot T}\right) \tag{10}$$

where σ_0 shows a pre-exponential coefficient, E_a is the energy of activation (eV), k shows the Boltzmann's constant (8.617×10^{-5} eV/K) and T is the absolute temperature.

A study has shown that doped ceria-based electrolytes exhibit electronic conductivity mainly at high temperatures (>1000 °C) [3]. Moreover, the oxide ion transference number of co-doped ceria electrolytes is close to 1 [23,24]. Therefore, the conductivity obtained from Eq. 9 is considered an ionic conductivity.

Figure 9 shows the Arrhenius' plot from 600 to 800 °C of BSDC electrolyte sintered at different temperatures. Arrhenius' plot states that for all the sintered pellets, the conductivity increases with the increase in temperature due to the increase in the mobility and decrease in the association enthalpy of the defects. Furthermore, the electrolyte sintered at 1200 °C exhibited the lowest conductivity because it showed high grain-boundary resistance throughout the whole temperature range (600 to 800 °C), due to the low relative density and high porosity compared with the pellets sintered at higher temperatures. As the sintering temperature increased, the value of conductivity increased but no significant difference was observed in the conductivity of the samples sintered at 1300 and 1400 °C, as given in Table 3, because both

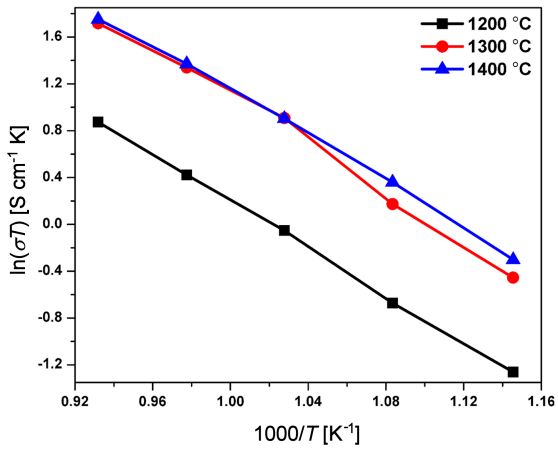

Figure 9. Arrhenius' plots of BSDC electrolyte sintered at different temperatures

Table 3. Ionic conductivity of BSDC sintered electrolytes at different temperatures

Sintering temperature [°C]	Ionic conductivity [S/cm] at different temperatures					Activation energy [eV]
	600 °C	650 °C	700 °C	750 °C	800 °C	700–800 °C
1200	0.0003	0.0006	0.0010	0.0015	0.0022	0.8324
1300	0.0007	0.0013	0.0025	0.0037	0.0052	0.7275
1400	0.0008	0.0016	0.0025	0.0038	0.0054	0.7633

of these samples had similar bulk resistance values as shown in Figs 7 and 8. However, at low temperature (650 °C), the electrolyte sintered at 1300 °C exhibited high grain-boundary resistance, as shown in Fig. 8. This happened since the grain boundaries were not so compact because of less densification at 1300 °C compared with 1400 °C. The activation energies of all the sintered pellets were calculated from the slopes of the Arrhenius' plot and are given in Table 3, and the sample sintered at 1300 °C shows lower activation energy at 700 to 800 °C.

The highest value of oxide ion conductivity at 800 °C for BSDC electrolyte was approximately 0.005 S/cm. This value is less than the reported values for co-doped ceria electrolytes [7,8,25]. This difference may be due to the small value of density (~87 %TD) for BSDC electrolyte even at 1400 °C compared with other co-doped electrolytes [7,25,26], because sintering of many ceramic materials to full density is difficult [16]. The other reason may be that co-doping of barium increases the ordering of oxygen vacancies and inhibited the ionic mobility due to the large ionic radius of Ba^{2+} (1.42 Å) compared to Ce^{4+} (0.97 Å). This large difference in ionic radii resulted in poor ionic conductivity of BSDC electrolyte system.

This study shows that $Ce_{0.8}Sm_{0.1}Ba_{0.1}O_{2-\delta}$ is not a prominent electrolyte material for oxide-ion conducting IT-SOFCs. Ba^{2+} is a potential candidate for the proton-conducting electrolyte systems [27–30]. However, the oxide ion conductivity of $Ce_{0.8}Sm_{0.1}Ba_{0.1}O_{2-\delta}$ electrolyte can be increased by enhancing densification via addition of sintering aids e.g., lithium oxide, like researchers did for other ceramic electrolytes [15]. We would determine the oxide ion conductivity of BSDC using different sintering aids in our future work.

IV. Conclusions

$Ce_{0.8}Sm_{0.1}Ba_{0.1}O_{2-\delta}$ co-doped ceria electrolyte was successfully synthesized by citric acid–nitrate combustion method. XRD analysis revealed that the electrolyte powder calcined at 900 °C for 5 h exhibited some secondary phases in the form of $BaCeO_3$ and $BaO_{1.3}$. However, all the major peaks were matched with the cubic fluorite crystal structure of CeO_2. FESEM analysis showed that the grain growth and densification increased with the increase in sintering temperature from 1200 to 1400 °C. The maximum relative density achieved was ~87 %TD at 1400 °C. An abnormal grain growth was observed at high sintering temperatures especially at 1400 °C. The oxide ion conductivity of BSDC electrolyte increased with the increase in sintering temperature. However, no appreciable change was observed in total conductivity as the sintering temperature increased from 1300 to 1400 °C. The sample sintered at 1300 °C showed the lowest value of activation energy i.e., 0.7275 eV at 700 to 800 °C. The $Ce_{0.8}Sm_{0.1}Ba_{0.1}O_{2-\delta}$ electrolyte showed an oxide ion conductivity of 0.005 S/cm at 800 °C. However, the addition of sintering aids may enhance its relative density, which consequently would increase its oxide-ion conductivity.

Acknowledgements: The work was supported by the Ministry of Science, Technology and Innovation Malaysia and the Universiti Kebangsaan Malaysia (UKM) via research sponsorships 03-01-02-SF1079, GUP-2016-045 and GUP-2015-038 and. The authors would like to acknowledge the support of Center for Research and Instrumentation Management (CRIM), UKM for excellent testing facilities.

References

1. S.C. Singhal, K. Kendall, *High Temperature Solid Oxide Fuel Cells: Fundamentals, Design and Applications*, Elsevier Ltd., UK, 2003.
2. R.P. O'Hayre, S.W. Cha, W.G. Colella, F.B. Prinz, *Fuel Cell Fundamentals*, John Wiley & Sons, Inc., New Jersey, 2009
3. G.B. Balazs, R.S. Glass, "AC impedance studies of rare earth oxide doped ceria", *Solid State Ionics*, **76** [1-2] (1995) 155–162.
4. Y-C. Wu, Y-Y. Liao, "Effect of Ca^{2+} and Sr^{2+} doping on the microstructure and cell performance of samaria-doped ceria electrolytes used in solid oxide fuel cells", *Int. J. Hydrogen Energy*, **41** [31] (2016) 13591–13602.
5. J. Yang, B. Ji, J. Si, Q. Zhang, Q. Yin, J. Xie, C. Tian, "Synthesis and properties of ceria based electrolyte for IT-SOFCs", *Int. J. Hydrogen Energy*, **41** [36] (2016) 15979–15984.
6. M. Kahlaoui, S. Chefi, A. Inoubli, A. Madani, C. Chefi, "Synthesis and electrical properties of co-doping with La^{3+}, Nd^{3+}, Y^{3+}, and Eu^{3+} citric acid-nitrate prepared samarium-doped ceria ceramics", *Ceram. Int.*, **39** [4] (2013) 3873–3879.
7. Y-C. Wu, C-C. Lin, "The microstructures and property analysis of aliovalent cations (Sm^{3+}, Mg^{2+}, Ca^{2+}, Sr^{2+}, Ba^{2+}) co-doped ceria-base electrolytes after an aging treatment", *Int. J. Hydrogen Energy*, **39** [15] (2014) 7988–8001.
8. X. Sha, Z. Lü, X. Huang, J. Miao, Z. Liu, X. Xin, Y. Zhang, W. Su, "Influence of the sintering temperature on electrical property of the $Ce_{0.8}Sm_{0.1}Y_{0.1}O_{1.9}$ electrolyte", *J. Alloys*

Compd., **433** [1-2] (2007) 274–278.
9. S.A. Muhammed Ali, R.E. Rosli, A. Muchtar, A.B. Sulong, M.R. Somalu, E.H. Majlan, "Effect of sintering temperature on surface morphology and electrical properties of samarium-doped ceria carbonate for solid oxide fuel cells", *Ceram. Int.*, **41** [1] (2015) 1323–1332.
10. C. Peng, Y. Zhang, Z.W. Cheng, X. Cheng, J. Meng, "Nitrate-citrate combustion synthesis and properties of $Ce_{1-x}Sm_xO_{2-x/2}$ solid solutions", *J. Mater. Sci. Mater. Electron.*, **13** [12] (2002) 757–762.
11. S.J. Hong, A.V. Virkar, "Lattice parameters and densities of rare-earth oxide doped ceria electrolytes", *J. Am. Ceram. Soc.*, **78** [2] (1995) 433–439.
12. M. Burbano, D. Marrocchelli, G.W. Watson, "Strain effects on the ionic conductivity of Y-doped ceria: A simulation study", *J. Electroceram.*, **32** [1] (2014) 28–36.
13. M.R. Kosinski, R.T. Baker, "Preparation and property-performance relationships in samarium-doped ceria nanopowders for solid oxide fuel cell electrolytes", *J. Power Sources*, **196** [5] (2011) 2498–2512.
14. Y-P. Fu, S-B. Wen, C-H. Lu, "Preparation and characterization of samaria-doped ceria electrolyte materials for solid oxide fuel cells", *J. Am. Ceram. Soc.*, **91** [1] (2007) 127–131.
15. G. Accardo, C. Ferone, R. Cioffi, "Influence of lithium on the sintering behavior and electrical properties of Ce0.8Gd0.2O1.9 for intermediate-temperature solid oxide fuel cells", *Energy Technol.*, **4** [3] (2016) 409–416.
16. W.D. Kingery, H.K. Bowen, D.R. Uhlmann, *Introduction to Ceramics*, John Wiley & Sons, New York, 1976.
17. M.N. Rahaman, *Ceramic Processing and Sintering*, Marcel Dekker Inc., New York, 1995.
18. L. Chen, D.F. Zhou, Y. Wang, X.F. Zhu, J. Meng, "Enhanced sintering of $Ce_{0.8}Nd_{0.2}O_{2-\delta}$-$La_{0.8}Sr_{0.2}Ga_{0.8}Mg_{0.2}O_{3-\delta}$ using CoO as a sintering aid", *Ceram. Int.*, **43** [4] (2017) 3583–3589.
19. J. Xiong, C. Jiao, M. Han, W. Yi, J. Ma, C. Yan, W. Cai, H. Cheng, "Effect of Li_2O additions upon the crystal structure, sinterability and electrical properties of yttria stabilized zirconia electrolyte", *RSC Adv.*, **6** [108] (2016) 106555–106562.
20. L. Zhang, F. Liu, K. Brinkman, K.L. Reifsnider, A.V. Virkar, "A study of gadolinia-doped ceria electrolyte by electrochemical impedance spectroscopy", *J. Power Sources*, **247** (2014) 947–960.
21. B. Ji, C. Tian, C. Wang, T. Wu, J. Xie, M. Li, "Preparation and characterization of $Ce_{0.8}Y_{0.2-x}Cu_xO_{2-\delta}$ as electrolyte for intermediate temperature solid oxide fuel cells", *J. Power Sources*, **278** (2015) 420–429.
22. K.C. Anjaneya, G.P. Nayaka, J. Manjanna, G. Govindaraj, K.N. Ganesha, "Preparation and characterization of $Ce_{1-x}Gd_xO_{2-\delta}$ (x = 0.1–0.3) as solid electrolyte for intermediate temperature SOFC", *J. Alloys Compd.*, **578** (2013) 53–59.
23. M. Dudek, "Some structural aspects of ionic conductivity in co-doped ceria-based electrolytes", *Arch. Metall. Mater.*, **58** [4] (2013) 1355–1359.
24. M. Dudek, M. Mroz, L. Zych, Drozdz-Ciesla, "Synthesis of ceria-based nanopowders suitable for manufacturing solid oxide electrolytes", *Mater. Sci. Pol.*, **26** [2] (2008) 319–329.
25. S. Banerjee, P.S. Devi, D. Topwal, S. Mandal, K. Menon, "Enhanced ionic conductivity in $Ce_{0.8}Sm_{0.2}O_{1.9}$: Unique effect of calcium co-doping", *Adv. Funct. Mater.*, **17** [15] (2007) 2847–2854.
26. Y. Liu, B. Li, X. Wei, W. Pan, "Citric-nitrate combustion synthesis and electrical conductivity of the Sm^{3+} and Nd^{3+} co-doped ceria electrolyte", *J. Am. Ceram. Soc.*, **91** [12] (2008) 3926–3930.
27. K. Singh, R. Kannan, V. Thangadurai, "Synthesis and characterisation of ceramic proton conducting perovskite-type multi-element-doped $Ba_{0.5}Sr_{0.5}Ce_{1-x-y-z}Zr_xGd_yY_zO_{3-\delta}$ ($0 < x < 0.5$; y = 0, 0.1, 0.15; z = 0.1, 0.2)", *Int. J. Hydrogen Energy*, **41** (2016) 13227–13237.
28. D.A. Medvedev, J.G. Lyagaeva, E.V. Gorbova, A.K. Demin, P. Tsiakaras, "Advanced materials for SOFC application: Strategies for the development of highly conductive and stable solid oxide proton electrolytes", *Prog. Mater. Sci.*, **75** (2016) 38–79.
29. Z. Shi, W. Sun, Z. Wang, J. Qian, W. Liu, "Samarium and yttrium codoped $BaCeO_3$ proton conductor with improved sinterability and higher electrical conductivity", *ACS Appl. Mater. Interfaces*, **6** [7] (2014) 5175–5182.
30. S.A. Muhammed Ali, M. Anwar, A.M. Abdalla, M.R. Somalu, A. Muchtar, "$Ce_{0.80}Sm_{0.10}Ba_{0.05}Er_{0.05}O_{2-\delta}$ multi-doped ceria electrolyte for intermediate temperature solid oxide fuel cells", *Ceram. Int.*, **43** (2017) 1265–1271.